Simultaneous dual-band entangled photon pair generation using a silicon photonic microring resonator

IOP Publishing Quantum Sci. Technol. 3 (2018) 034001 https://doi.org/10.1088/2058-9565/aab89a

Quantum Science and Technology

OPEN ACCESS

RECEIVED
5 December 2017

REVISED
2 March 2018

ACCEPTED FOR PUBLICATION
22 March 2018

PUBLISHED
11 April 2018

PAPER

Simultaneous dual-band entangled photon pair generation using a silicon photonic microring resonator

Chaoxuan Ma and Shayan Mookherjea

University of California, San Diego, Department of Electrical and Computer Engineering, La Jolla, CA 92093-0407, United States of America

E-mail: smookherjea@ucsd.edu

Keywords: quantum communication, dual-band, entangled photons, silicon microring

Abstract

Traditional entangled photon pair generation apparatus, such as periodically-poled nonlinear crystals or microstructured fibers, require special and complex device structures to permit spontaneous nonlinear interactions at different wavelengths to occur simultaneously. This makes it difficult to design a single device that can, for example, generate high-quality, high-brightness photon pairs at both the 1310 and 1550 nm wavelength bands. Such flexibility will be useful in reconfiguring quantum communications to co-exist with data and telecommunications networks in popular use today. We show that a simple, appropriately-designed silicon microring device can achieve this objective, and explain the design and measurements of photon pair generation including coincidences-to-accidentals ratio and Franson interferometry of energy–time entanglement.

1. Introduction and motivation

The innovation discussed in this paper is the design and measurement of a silicon photonic microring resonator which can generate high-quality energy–time entangled photon pairs simultaneously at the 1310 and 1550 nm wavelength bands. Since these are the two spectral bands which are widely used in classical communications, a pair generation device should ideally be able to operate in both spectral ranges where initial applications of quantum communication (e.g., quantum key distribution) may be implemented. Moreover, an argument has been made, in the context of fiber experiments, for generating and using quantum photons at 1310 nm [1, 2] which is less widely studied than the 1550 nm band. Before discussing the technical details of this advancement, we first present a brief motivation of the problem.

Optically-pumped unseeded nonlinear processes, such as spontaneous parametric down-conversion (SPDC) and spontaneous four-wave mixing (SFWM), are one of the main ways to generate entangled photon pairs as a resource for quantum communication, fundamental physics experiments, and other applications [3]. Traditional entangled photon pair generation devices are formed using optical fiber [4] or crystals such as periodically-poled lithium niobate (PPLN), potassium trihydrogen phosphate (KTP), lithium tantalate etc [5–9]. Crystals themselves have a wide transparency range, and can be used at various wavelength ranges including visible, near-infrared and portions of the mid-infrared spectrum as well. In crystals, the generation of photon pairs at both bands simultaneously and without cross-correlations has not been shown. Operation at distinctly different wavelength bands in the same device is difficult, since periodically-poled gratings phase-match efficiently over only a narrow band of wavelengths, and gratings, in general, have higher-order resonances that may scatter light and impair the performance.

The last ten years have witnessed the development of silicon photonic approaches to generating entangled photon pairs [10–21]. Some of the most important advantages are technological: silicon volume manufacturing using wafer-scale technology can be inexpensive, and silicon photonic devices can be integrated with lasers [22] and/or detectors [23]. Other important advantages are fundamental: The intrinsic rate of nonlinear optical processes increases as the mode volume decreases, which reduces the pump power requirements of high core-cladding index contrast silicon microrings used for pair generation to sub-milliwatt levels [18], and the device

footprint to about one hundred square-microns [11, 12]. To explain why micro-resonators are very useful in the silicon photonics approach to pair generation, we recall that because of the third-order nonlinearity used in SFWM (compared to the second-order nonlinearity used in SPDC), silicon photonic waveguide devices generate photon pairs at a low rate compared to PPLN or PPKTP waveguides. However, this can be partly mitigated by sacrificing continuously-broadband wavelength coverage, and using resonant devices with high-quality (Q) factors. Indeed, silicon photonic microring resonators can now generate MHz-rate entangled pairs of high quality with milliwatt-scale pump powers [24]. Moreover, silicon device technology is useful not only for the optical components but the necessary micro-electronics needed to make a working system, e.g., monitoring the optical micro-resonators [25, 26], and incorporating electro-optic modulators and switches [27–29] as a step towards full integration.

For quantum communications using integrated photonics components, it is not yet clear which spectral band is preferred in the deployed fiber links where both C/L-band (approximately 1530–1600 nm) and O-band (1310 nm) wavelengths are used. Some communications schemes, such as passive optical networks, use both wavelength bands [30]. As discussed in [31], the Raman noise incurred in fiber propagation at 1310 nm wavelengths can be significantly (about 4000 times) weaker than at 1550 nm; however, the propagation loss (fiber attenuation) can be higher. In terms of device technology, there are more WDM components (splitters, filters, MUX/de-MUX etc) available at 1550 nm, but the standard channel spacing at 1310 nm (O) Band is wider, making filtering easier, which is one of the most challenging requirements for integrated photonics. Thus, it is not clear which is the preferred wavelength regime for operation of a microchip pair-source intended for compatibility with short-distance fiber communications. The detector efficiency of single-photon detectors, particularly, avalanche diode detectors, also varies strongly with wavelength, and dark-count reduction may be achieved by operating in the O-band. Hence, researchers have developed pair sources at both wavelengths, for example [32] in the C-band and [33] at the O-band.

In fact, devices using SPDC can generate a photon pair with one photon at 1550 nm and the other at 1310 nm, and thus, one photon can serve as the herald for the other [34–37]. While this is not possible in silicon photonics because of the comparatively-narrow band nature of SFWM phase-matching, we demonstrate that a single microring resonator can, in fact, generate entangled photons of high quality at each wavelength band separately. This is not an obvious result, in the sense that the modal properties of silicon nanophotonic waveguides, and the coupling behavior of micro-resonators to waveguides, are strongly wavelength-dependent in high-index-contrast silicon photonics [38]. The use of a single device which can operate at either wavelength regime, as desired, is important to reduce the device fabrication/yield variability, which is still a significant concern in foundry-fabricated silicon photonics, especially with high-Q micro-resonators that require an optimized coupling to a waveguide for optimum operation [18].

Here, we address one of the existing limitations of silicon photonic pair generation devices: the difficulty in generating high-quality entangled photon pairs at both of the 1.3 and 1.55 μm wavelength bands that are widely used in optical communication networks and components. In this report, a simple device is measured and characterized which generates a high quality of entangled photon pairs at both these wavelengths *simultaneously*, when two optical pumps are introduced. The structure also works as a 'regular' pair generation device when only one pump is used, and in fact, one of the measurements reported here is that of a coincidences-to-accidentals ratio (CAR) of 19 000 which is the highest CAR value yet reported for silicon photonics pair generation in any device, at any wavelength.

Moreover, by separating the two pump wavelengths by more than 200 nm, this device helps meet the ongoing challenges of multiplexing and scaling up photon pair generation, and avoid the difficulties and impairments (such as cross-pump interactions) faced in two pump SFWM processes when the two pump wavelengths are close to each other [39].

The underlying technical challenge is to design a silicon photonic pair generation structure that can operate at these rather different wavelengths. Firstly, compared to diffused/ion-exchanged waveguides in glass, or optical fiber, the group velocity dispersion of silicon waveguides is very high (by three or four orders of magnitude). Thus, not only is a Si waveguide much less efficient than a PPLN waveguide, but it is more dispersive as well. Secondly, dual-band micro-resonators with a clean transmission spectrum (showing suppression of multi-mode effects) are uncommon (but, as shown here, not impossible), since components, materials and cross-sections are typically optimized around one wavelength.

What is required is six-fold resonance at pump, Stokes (also called 'idler'), and anti-Stokes ('signal') wavelengths of SFWM process at both bands, which would be very difficult to design and to operate in a stable manner for traditional nonlinear resonator devices using III–V semiconductors [40] or periodically-poled crystal waveguides. As shown here, the high-index contrast of silicon photonics, coupled with the ability of silicon microfabrication techniques which allow for precise and repeatable fabrication, results in devices that show clean, essentially single-mode transmission spectra at both 1310 and 1550 nm wavelength bands. Also, the ability of silicon (a semiconductor) to incorporate microelectronic components such as monitoring p-i-n diodes

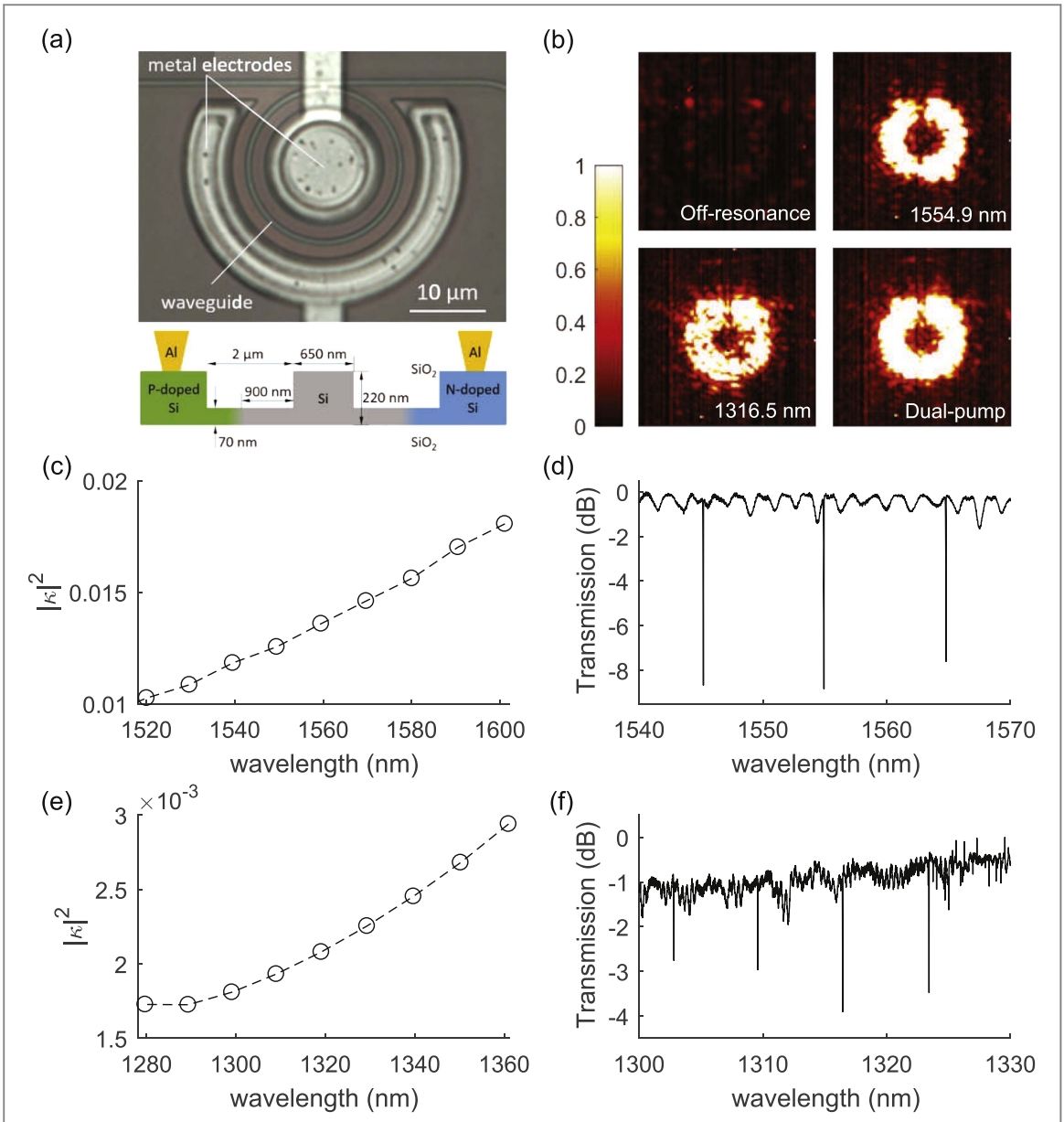

Figure 1. (a) Upper: microscope image of the ring resonator side-coupled to a waveguide, with metal traces connecting to a p-i-n diode fabricated across the microring to monitor its resonance [25]. Lower: a schematic of the waveguide section. Figure reproduced from [25], with the permission of AIP Publishing. (b) Infrared camera images, acquired using a top-view microscope and a high-magnification objective lens, of the microring off-resonance and resonating with 1554.94 nm pump light, with 1316.52 nm pump light, and with both wavelengths simultaneously. (c) and (e) are FDTD-simulated coupling efficiency calculations $|\kappa|^2$ as a function of wavelength at 1550 nm and 1310 nm bands respectively. (d) and (f) are the measured transmission spectra at 1550 nm and 1310 nm bands, respectively, showing a single-mode-family set of resonances at both bands in the same device.

within the microring itself allows for monitoring and alignment of the resonance to the pump wavelengths, was essential for stable operation and the measurements reported here.

2. Microring design and characterization

The simple device used for simultaneous dual-band entangled photon pair generation is a high-quality factor (Q) microring, side-coupled to a single waveguide (i.e., the so-called 'all pass' configuration), with an appropriately-chosen coupling coefficient as described below. A microscopic image of the ring resonator together with a schematic of the waveguide cross-section is shown in figure 1(a). The microchip was fabricated using a foundry silicon photonic process on silicon-on-insulator wafers, using ridge waveguides of width 0.65 μm, height 0.22 μm, and slab thickness 70 nm, designed for low loss transmission in the lowest-order (i.e., fundamental) mode of the transverse electric (TE) polarization defined relative to the device plane. The

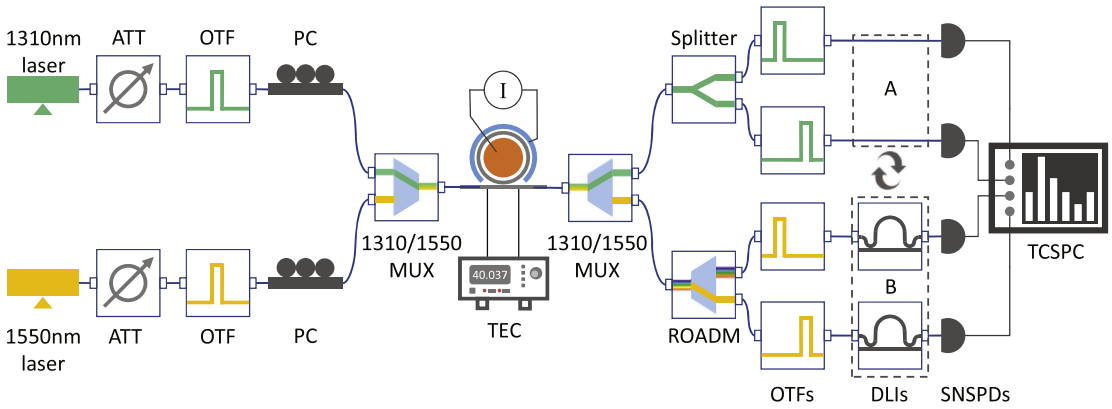

Figure 2. Experimental setup for pair generation and measurements of the cross-correlation between signal and idler photons i.e., the coincidences-to-accidentals ratio (CAR), and two-photon Franson interferometry visibility. For the CAR measurement, all the SNSPDs connected directly to the filters (Box B was replaced by another Box A). For the visibility measurement, Box B was used to measure the fringe visibility of photon pairs generated by one pump, as described in the text, while Box A simply connected filters and detectors to monitor the photon count rates generated by the other pump and measure their CAR. ATT: variable optical attenuator, OTF: optical tunable filter, PC: polarization controller, MUX: multiplexer, TEC: thermoelectric controller, ROADM: 3-port reconfigurable optical add-drop multiplexer, DLI: delay-line interferometer, SNSPD: superconducting nanowire single-photon detector, TCSPC: time-correlated single-photon counter.

microring had a radius $R = 10\ \mu$m. The slab regions of the ridge waveguides were doped, followed by contact and via formation and metalization, to form a p-i-n diode for monitoring, under reverse bias, the optical power circulating in the microring.

Here, the coupling coefficient (κ) between the microring and the waveguide is defined as the length-integrated scalar coefficient that appears in the matrix formulation of resonator-waveguide coupling summarized elsewhere [41]. Simulations of $|\kappa|$ versus wavelength (λ) at both the 1550 nm and 1310 nm wavelength bands are shown in figures 1(c) and (e), respectively, for the lowest-order quasi TE polarized electrical field. A small value of $|\kappa| \ll 0.05$ is one of the two necessary components for achieving a high loaded Q-factor, and thereby, bright pair generation, with the other factor being the loss of the waveguide.

The silicon waveguides used in the feeder waveguide and microring had a propagation loss (measured on test sites consisting of waveguides of different lengths) of approximately 0.74 ± 0.02 dB cm^{-1} at 1550 nm and 1.13 ± 0.12 dB cm^{-1} at 1310 nm, resulting in: (a) at 1550 nm, an intrinsic Q-factor of approximately 9×10^5, and a resonance lifetime $\tau \approx 76$ ps (loaded Q-factor of 9.2×10^4, with a spectral full-width at half-maximum (FWHM) of approximately 2.1 GHz); and (b) at 1310 nm, an intrinsic Q-factor of approximately 3×10^5, and a resonance lifetime $\tau \approx 40$ ps (loaded Q-factor of 5.7×10^4, with a spectral FWHM of approximately 4.0 GHz). A 'clean' transmission spectrum was measured at both wavelength bands, as shown in figures 1(d) and (f). Recall that the overall Q-factor depends on both the intrinsic propagation loss of the waveguide forming the microring and the coupling coefficient between the microring and the waveguide. Here, the slightly higher propagation loss at 1310 nm is somewhat compensated for by the smaller waveguide-to-ring coupling coefficient, as shown in figures 1(c) and (e). Thus, a similarly high Q-factor is achieved at both wavelength bands.

Photon pair generation measurements reported here used the experimental configuration shown in figure 2. The bare-die chip was mounted on a temperature-controlled stage with a thermoelectric controller in feedback with a thermistor on the stage mount. The spectral alignment of the pump laser(s) to the microring was continuously monitored during measurement using the reverse-biased photo-current of a silicon p-i-n junction diode fabricated across the microring [25], and confirmed using high-magnification infrared camera images of the microring. Figure 1(b) shows infrared camera images of the microring at the resonance conditions of the two pump lasers, operated individually and also simultaneously. Because of the limited dynamic range of the camera, it was difficult to quantitatively distinguish the third case from the first two; however, the photo-current readout with two pump lasers was seen to be a linear sum of the photocurrents for the two individual lasers. A readily-detectable photo-current (in the micro-ampere range, at a reverse bias of 1 V) was provided by the silicon waveguide comprising the ring without ion-implantation or defect-enhancement of the waveguide, or the introduction of other materials such as germanium or III–V semiconductors.

Light was coupled to and off the silicon chip using polarization-maintaining fibers, polarization controllers, and lensed tapered fibers with anti-reflection coating. The latter was designed for C-band, but functional for O-band as well. The insertion loss of each fiber-to-waveguide coupler was estimated as 3.5 dB. Nanopositioning stages with piezoelectric actuators were used for accurate positioning of the fiber tips to the waveguide facets. Input light from the O-band and C-band pump wavelengths, after filtering out the amplified spontaneous

emission (ASE) background with a relatively broad bandpass filter (FWHM of 1.8 nm at 1310 nm and 1 nm at 1550 nm), was combined using a wavelength-division multiplexing (WDM) fiber component. An identical WDM component was used to spectrally separate the output light at the chip output, which was then routed through cascaded filters to select one pair of spectral lines of Stokes and anti-Stokes photons positioned symmetrically around each pump wavelength.

Under SFWM, energy-conservation between the pump and the generated Stokes and anti-Stokes photon pair dictates the frequency relationship, $2\omega_p = \omega_S + \omega_{aS}$, and the range of frequencies over which this occurs is limited to a few terahertz (around each pump frequency) because of the dispersion of the coupler and the waveguides. In each band, the same microring provided simultaneous resonance for all three frequencies across adjacent free-spectral ranges with a tight constraint on the narrow bandwidth dictated by the high-Q resonance.

We used commercially available, telecommunications grade fiber-coupled optical filters for these measurements. Two distinct sets of filters were used for the 1310 and 1550 nm bands; in the latter case, the availability of reconfigurable optical add-drop multiplexers (ROADMs) made the experimental setup more versatile, as shown in figure 2. ROADMs are not yet readily available at the 1310 nm wavelength band, and we simply used a 3 dB splitter to separate the 'signal' and 'idler' photons, incurring a penalty in the coincidence rate. In the 1310 nm wavelength band, the pump wavelength was positioned at 1316.5 nm and signal and idler photons were detected at 1309.8 nm and 1323.1 nm, respectively, with filter FWHM's of approximately 1.8 nm at both wavelengths. In the 1550 nm wavelength band, the pump wavelength was positioned at 1554.9 nm and signal and idler photons were detected at 1535.5 nm and 1574.7 nm, respectively, with filter FWHM's of approximately 0.6 nm and 0.8 nm, respectively. Next-to-nearest resonances are chosen here for pair generation in 1550 nm band due to the limited wavelength tuning ranges of the filters, which are 1528–1562 nm for C-band filters (for signal photons) and 1567–1603 nm for L-band filters (for idler photons). Note that the spectral width (FWHM) of the microring resonance was approximately 0.03 nm, much narrower than any of the filter widths. Thus, these filters do not reshape the joint-spectral intensity, as may be a concern with broadband SFWM in waveguides.

Photons were detected using four fiber-coupled superconducting (WSi) nanowire single-photon detectors (SNSPD), cooled to 0.8 K in a closed-cycle Helium-4 cryostat equipped with a sorption stage. Two detectors were optimized for wavelengths around 1310 nm with a detection efficiency of 90%, and the other two for 1550 nm with 65% detection efficiency. These detectors were not gated and operated in a simple DC-biased mode with an RF-amplified readout. Coincidences were measured using a multi-input time-to-digital converter instrument, with 0.08 ns minimum bin width, in start-stop mode. To prevent binning artifacts when accumulating histograms, at the cost of a factor of two in temporal resolution, two adjacent hardware bins were summed, according the manufacturer's suggestions, resulting in the 0.16 ns bin width used for all coincidence measurements. Previously, we have also measured coincidence histograms using a two-channel time-correlated single-photon counting instrument with 25 ps bin size, which gave similar results in terms of the shape and widths of the coincidence peaks.

3. Measurements and analysis

The silicon microring generated photon pairs at both wavelength bands separately, and also at both bands simultaneously when excited by both pumps. Continuous-wave pumps were used for all these experiments. Before discussing the quality of the photon pairs, we first discuss the dynamics when the second optical pump is turned on and off, in the presence of the first pump. This is shown in figure 3, which recorded the change in single counts of all four channels (1550 nm signal and idler, 1310 nm signal and idler) when the pumps were turned on and off individually. First, each pump was positioned (i.e., the numerical values of the laser wavelength and power settings were chosen) individually and separately. Next, to create the time-resolved graph shown in figure 3, the second pump was simply turned on (at the pre-determined wavelength power settings, with no further adjustment) when the first pump was already active. Next, the first pump was turned off, and then it was turned back on etc again with no wavelength or power tuning. This mimics the operation of the device in a practical communication network setting, where fine-tuning of the resonance may not be practical.

The p-i-n diode fabricated across the waveguide cross-section was used to monitor the resonance of the microring to the laser wavelength(s), as described elsewhere [25]. A reverse bias of −1 V was used to generate a small but easily-measured photo-current, in the micro-ampere range, when the pump light circulated in the resonant microring, whereas the dark photo-current readout was in the nano-ampere range (i.e., approximately 30 dB dynamic range).

Under these conditions, figure 3 shows an anti-correlation between the photon pair fluxes generated by the two pumps, i.e., the photon generation rate at 1550 nm drops slightly when the 1310 nm pump is turned on, and

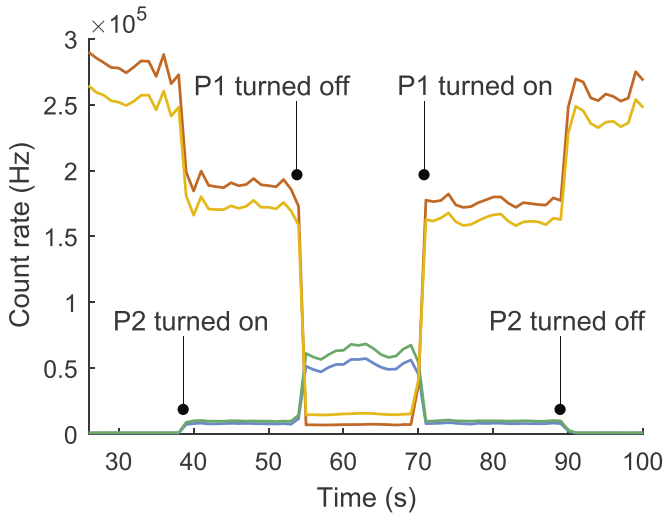

Figure 3. Measured singles count rates as the second pump is turned on and off, after the first. *P*1 and *P*2 are 1550 nm and 1310 nm pumps respectively. Red and yellow lines are single counts for 1550 nm signal and idler photons; green and blue lines are those for 1310 nm signal and idler photons.

the photon generation at 1310 nm rises further when the pump at 1550 nm is turned off etc. Finite numbers of counts were registered on the 1550 nm detectors from the 1310 nm pumps alone, but there was negligible signal-idler cross-correlation in this regime (and no entanglement), so these residual photons are just a noise background from the ASE of the 1310 nm pump laser leaking through the filters, and do not serve any purpose (or leak any information about the 1310 nm correlated-photon pair).

The anti-correlation behavior seen in figure 3 is more likely to be caused by a minor shifting of ring resonances induced by heating of micro-resonator when a second pump is added, alongside the residual (the p-i-n diode is operated with a reverse bias) free-carrier absorption and nonlinear two-photon absorption, rather than pump-pump mixing or depletion. The measured reverse-biased photocurrents across the p-i-n diode in the waveguide cross-section, which measure the pump powers coupled into the micro-resonator, was, in the combined pump case (5.3 μA), approximately equal to the sum of the photocurrents in the individual pump cases (4.6 μA for the 1310 pump of −4 dBm alone and 0.7 μA for the 1550 pump of −6 dBm alone). Future measurements are being planned to investigate the time-constant of the change induced by turning one of the two pumps on and off, but it appears to be relatively slow. The magnitude and sign (i.e., positive or negative change) of the variations shown in the figure depend on the precise tunings of the wavelengths and their positioning on the red or blue side of the 'cold-cavity' resonance. Theoretically, the optimal positioning of multiple optical pumps in a semiconductor microring resonator which exhibits thermally- and carrier-driven bistability is a complex problem to be addressed separately from this experimental paper, which shows that even without careful fine-tuning of the wavelengths and pump powers, the microring can generate entangled photons at both pump wavelengths.

To characterize the photon pairs, we examined the conventional pair-wise metrics such as the CAR, which, for high values of CAR, is basically equal to the second-order cross-correlation at zero time difference between the signal and idler photons, and also the two-photon Franson interferometric visibility for energy–time entanglement [3]. Again, pump wavelengths are pre-determined without re-positioning in these measurements. Since there are two pumps, we examine not only the anticipated pairs (e.g., the signal and idler photons at the 1550 nm band only, or the signal and idler photons at the 1310 nm band only), but also the cross-correlations across wavelength bands (e.g., selecting a signal photon from the 1310 nm band and the idler photon from the 1550 nm band, and vice versa).

3.1. Coincidences-to-accidentals ratio (CAR)

Figure 4 shows the second-order signal-idler cross-correlation function, $g_{SI}^{(2)}(\tau)$, between the signal (S) and idler (I) photons, measured across all the various pair-wise combinations of 'S' and 'I' channels, i.e., selecting an 'S' from either the 1550 nm band (subscript labeled '*a*') or the 1310 nm band (labeled 'α'), and similarly for the 'I' photon (labeled '*b*' and 'β', respectively). The measurements shown in figure 4 were performed when both pumps are present, with c.w. power levels of −4 dBm at 1310 nm and −6 dBm at 1550 nm, measured in the optical fiber just before the chip.

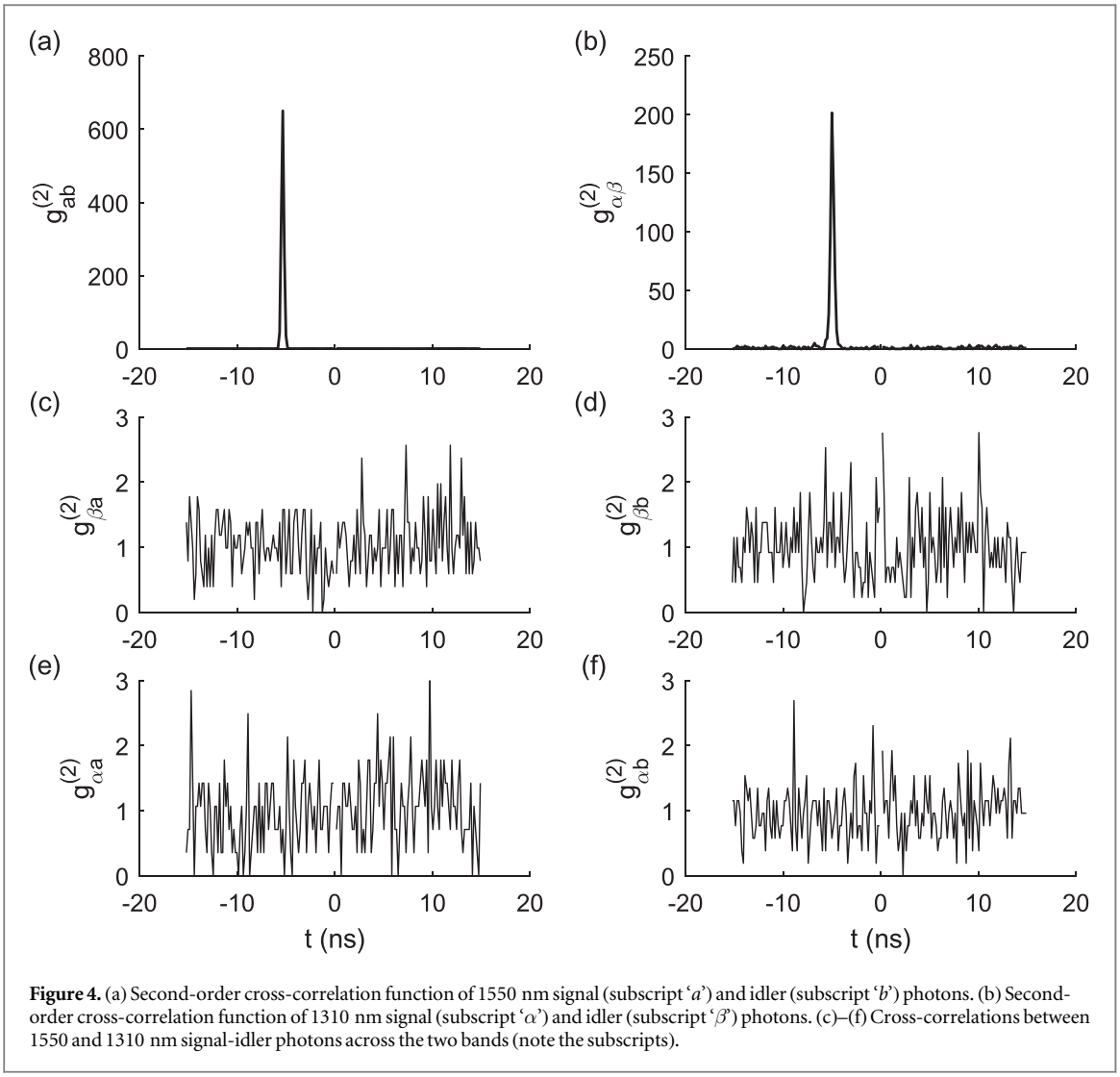

Figure 4. (a) Second-order cross-correlation function of 1550 nm signal (subscript '*a*') and idler (subscript '*b*') photons. (b) Second-order cross-correlation function of 1310 nm signal (subscript 'α') and idler (subscript 'β') photons. (c)–(f) Cross-correlations between 1550 and 1310 nm signal-idler photons across the two bands (note the subscripts).

The 'in-band' cross-correlation $g^{(2)}{}_{ab}(\tau)$ between the 1550 nm signal and idler photons (figure 4(a)), and the 'in-band' cross-correlation $g^{(2)}_{\alpha\beta}(\tau)$ between the 1310 nm signal and idler photons (figure 4(b)) each exhibits a clean sharp peak. The value of this peak is approximately equal to 1 + CAR. The figures clearly indicate a strong correlation between signal and idler photons originated from the same pump. Figures 4(c), (d) show no evidence of cross-correlation when the signal and idler photons are selected from among the pairs generated by different pumps, e.g., a signal photon from the 1550 nm SFWM process and an idler photon from the 1310 nm SFWM process. These are indeed the result we expect and desire, and they indicate that, in this device, each SFWM process operates independently and in parallel. Moreover, since the wavelengths of the pumps were not changed when the second pump was added to the first, these results also show that this silicon microring, as designed, was not too strongly perturbed (e.g., detuned, or its *Q*-factor degraded) when the second SFWM process was added to the first.

To study this phenomenon in more depth, and explain why the microring works satisfactorily at both wavelength bands, $g^{(2)}_{\mathrm{SI}}(\tau)$ was measured for a signal-idler photon pair generated by the 1550 nm pump, at a sequence of pump power levels, and in the presence of a 1310 nm pump with c.w. power level −4 dBm in the fiber before the chip, also performing its own SFWM process. Each peak was fitted by a Gaussian function, whose FWHM was typically 0.31 ns (which is the expected value for the settings and detectors used in this experiment). The resulting $g^{(2)}_{\mathrm{SI}}(0)$ as a function of input pump power at the 1550 nm wavelength band is shown in figure 5. When $g^{(2)}_{\mathrm{SI}}(0)$ continues to increase at low pump power (P), as shown by the data points in figure 5(a), a fitted line was used with the functional form aP^{-b}, where a and b are constants. When $g^{(2)}_{\mathrm{SI}}(0)$ saturates, and then decreases (because of fewer measured true coincidences compared to accidentals) at small values of P, as shown by the data points in figure 5(b), a fitted line was used with the functional form $(aP^2 + bP + c)^{-1}$, similar to those used in [13, 42]. In such cases, there is an additional noise contribution to the denominator of the CAR expression, whether from Raman noise [42], detector dark counts [13] or imperfect pump ASE extinction (here).

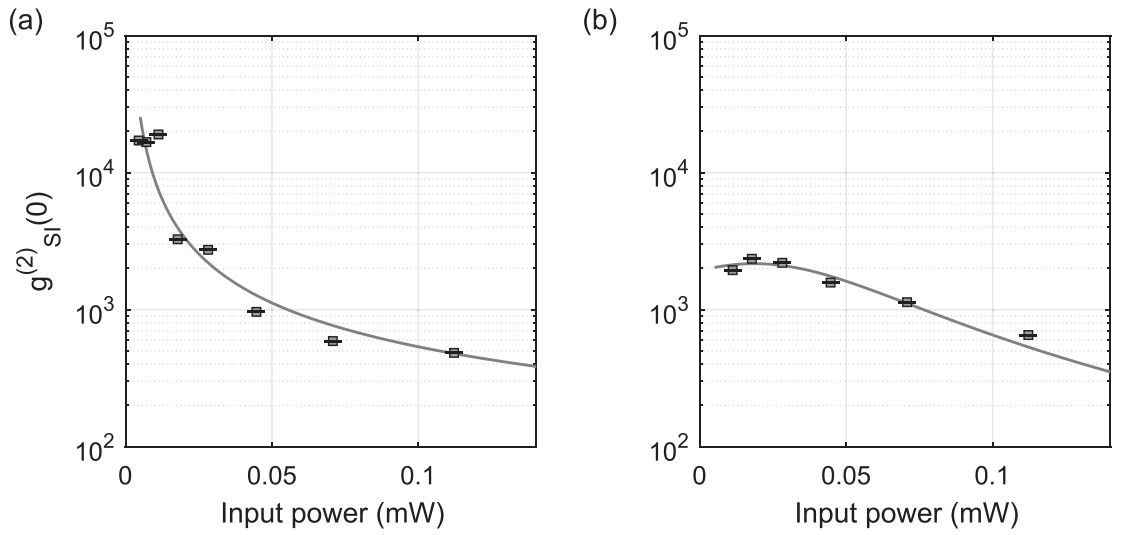

Figure 5. Second-order signal-idler cross-correlation at zero time difference (essentially equal to 1 + CAR, coincidences-to-accidentals ratio) as a function of input pump power (at 1550 nm) in the feeder waveguide before the microring when (a) only 1550 nm pump is present; (b) both 1550 and 1310 nm pumps are present.

However, in the earlier reports, the highest values of CAR were much less than 100, whereas the limit here is higher. Acquisition time for each measurement ranges from a few seconds to a few minutes, depending on the input pump power level, since longer acquisition time is required to obtain a small uncertainty error bar. The uncertainties, too small to see in the figures, are mainly from accidentals (broken pairs from the losses incurred in coupling off the chip and subsequent filtering) and are calculated as one standard deviation in the values of $g^{(2)}(\tau)$ in bins away from the peak.

When only the 1550 nm pump was present, we measured a very high $g^{(2)}_{SI}(0)$ value, 19 001 $\pm$ 144, resulting in a CAR of 19 000 which is the highest CAR value yet reported for silicon photonics pair generation in any device, at any wavelength. As is usual, this occurs at the lower end of the range of pump powers used in the experiment, when the measured (i.e., including the coupling and filtering losses) singles rates were 2 and 1.7 kHz, and loss-scaled (on-chip) photon generation rates were 37 and 56 kHz. At the highest power value used here, with the 1550 nm pump set to c.w. power level −6 dBm in the fiber before the chip, $g^{(2)}_{SI}(0)$ was 484 $\pm$ 4, for which case the measured singles rates were 50 and 46 kHz, and the on-chip photon generation rates were 0.93 and 1.5 MHz for the signal and idler photons. In passing, we note that these values are similar (CAR of 532 at a pair generation rate of 1.1 MHz) to those tabulated in our recent experiment focusing on the 1550 nm SFWM process only [24], in which we further showed a Hanbury-Brown and Twiss measurement with conditional self-correlation, $g^{(2)}_{ss}(0) = 0.098$ i.e., strong anti-bunching of a heralded single-photon source.

The same measurements were performed when the 1310 nm pump (power −4 dBm before the chip) was also present, whose SFWM process resulted in measured singles rates of 48 and 54 kHz, corresponding to on-chip photon generation rates of 1.6 and 2.3 MHz. In this case, $g^{(2)}_{SI}(0)$ again increased at lower power levels (of the 1550 nm pump), but saturated at about 1943 $\pm$ 15 while still obtaining a high value of 653 $\pm$ 5 at the maximum power value. Thus, the CAR values are similar at the higher power levels (and at megahertz-rates of generated photons), but we were able to reach a higher CAR value at the lower power levels (and few-kilohertz-rates of generated photons) when only the 1550 nm pump was used, rather than both pumps. This is most likely due to a small value of residual pump power from the ASE of the 1310 nm pump leaking through the finite extinction ratio of the filters, and causing a small number of accidental counts which are more strongly felt when the number of true coincidences is low.

3.2. Energy–time entanglement

The generated photon pairs from both pumps are expected to demonstrate energy–time entanglement which can be investigated through a Franson-type two-photon interference experiment, by violating Bell's inequality [43, 44]. Such measurements have already been shown (at a single wavelength, rather than the simultaneous SFWM process occurring here) for several silicon photonic pair generation devices [45–50].

We use the unfolded Franson interferometer configuration as shown in figure 2, in which an electronically-tunable delay-line interferometer (DLI, also known as an unbalanced Mach–Zehnder interferometer) is placed in the pathway of each of the signal and idler photons of the generated pair (after filtering). The two DLI's used in

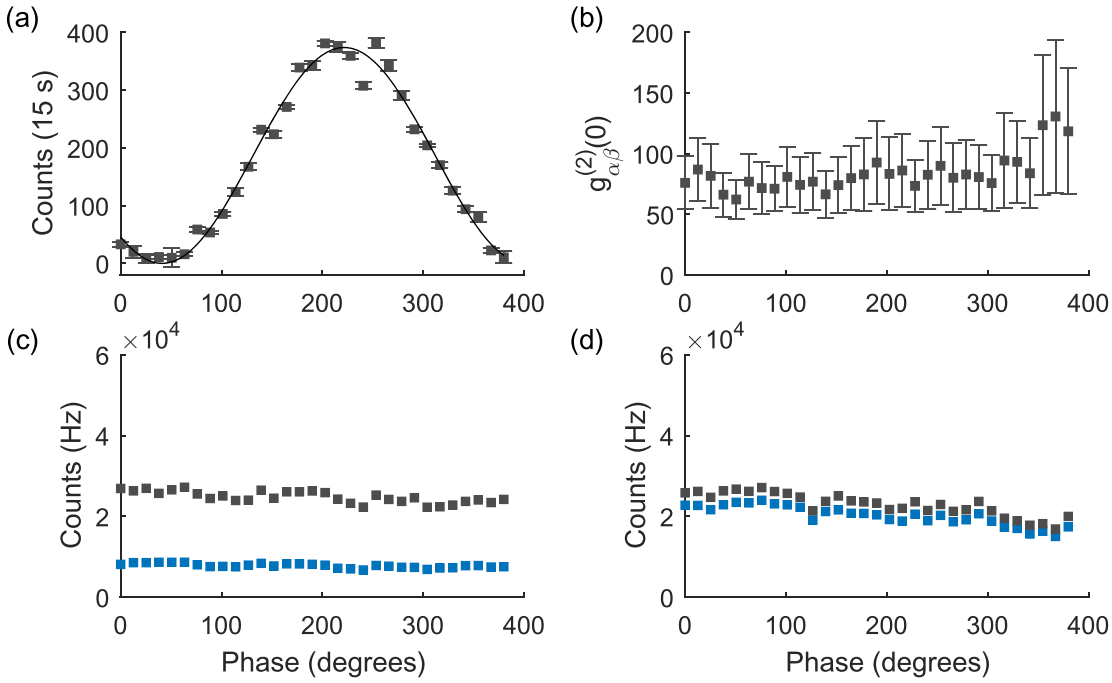

Figure 6. Time–energy entanglement measurement of 1550 nm photon pairs at presence of 1310 nm pump. (a) Franson visibility fringe of the 'short–short' and 'long–long' coincidence interference for photons pairs generated near 1550 nm. The horizontal axis corresponds to a phase setting of the delay-line interferometer, obtained by scaling the step-scanned experimental voltage setting by the voltage required to achieve a 2π phase shift. (b) Second-order cross-correlation function, related to the CAR for photon pairs generated near 1310 nm. (c) Measured singles count rates for signal and idler photons near 1550 nm. (d) Measured singles count rates for signal and idler photons near 1310 nm.

these measurements were fiber-coupled, polarization-maintaining devices, each with an FSR of 2.5 GHz (at 1550 nm) and peak-to-valley extinction ratio approximately 25 dB. Although designed for the 1550 nm wavelength (i.e., the manufacturer-specified FSR and insertion loss is correct at 1550 nm), we verified that they can also be used at 1310 nm with low insertion loss, but a different FSR (which is irrelevant for these measurements). The phase difference in the DLI's was piezo-controlled, and was tuned by voltage from a programmable low-noise power supply. Unlike in other experiments [49, 50], no active DLI stabilization was required. Such DLI's are costly, individually-assembled instruments and we have two DLI's available for experiments. Thus, when the Franson measurement was performed at 1550 nm (i.e., photon pairs generated in the 1550 nm band were routed through the DLI's), a CAR measurement was simultaneously performed at 1310 nm. Similarly, when the Franson measurement was performed at 1310 nm, a coincidences-to-accidentals measurement was simultaneously performed at 1550 nm.

The visibility fringes were measured by step-scanning the voltage setting on one DLI and holding it constant on the other DLI. A start-stop histogram was recorded for each voltage setting, and the histogram shows three peaks (as usual): the outer peaks correspond to the 'short-long' and 'long-short' coincidences (i.e., one of the photons goes through the short arm of its DLI and the other goes through the long arm of its DLI). The amplitude of these peaks do not change with phase tuning of the DLI's. The central peak consists of the interference of the 'short–short' and 'long–long' paths, whose peak amplitude, being a superposition of two interfering pathways, varies sinusoidally with the phase difference between the two DLI's, i.e., with the voltage setting. The fitting uncertainty (one standard deviation) is shown as the error bar in figures 6(a) and (b) and is too small to be visible. Although the signal and idler photons are at different wavelengths, separated by about 40 nm, the differential group delay accumulated over a few meters of fiber is negligible, compared to the timing jitter of the detectors.

The ring was pumped at both 1550 nm and 1310 nm, with power of −6 dBm and −4 dBm before the chip respectively. Measurement results for 1550 nm photons are shown in figure 6. The vertical axis corresponds to the measured number of coincidences in the indicated time interval, without scaling for the losses incurred in off-chip coupling, filtering and the finite detection efficiency. The observed fringe in figure 6(a) shows a fitted visibility of 97.8 ± 4%, which clearly surpasses the 71% visibility necessary for violation of Bell's inequality [43, 44] (without necessarily providing a test of local realism) as proof of photon pair time–energy entanglement. The uncertainty in the visibility value derives from the goodness-of-fit of the sinusoid function, while those for each data point, too small to be visible here, stem from goodness-of-fit of the fitted parameters of the Gaussian function used to fit the central coincidence peak. Figure 6(b) shows the signal-idler cross-correlation at zero

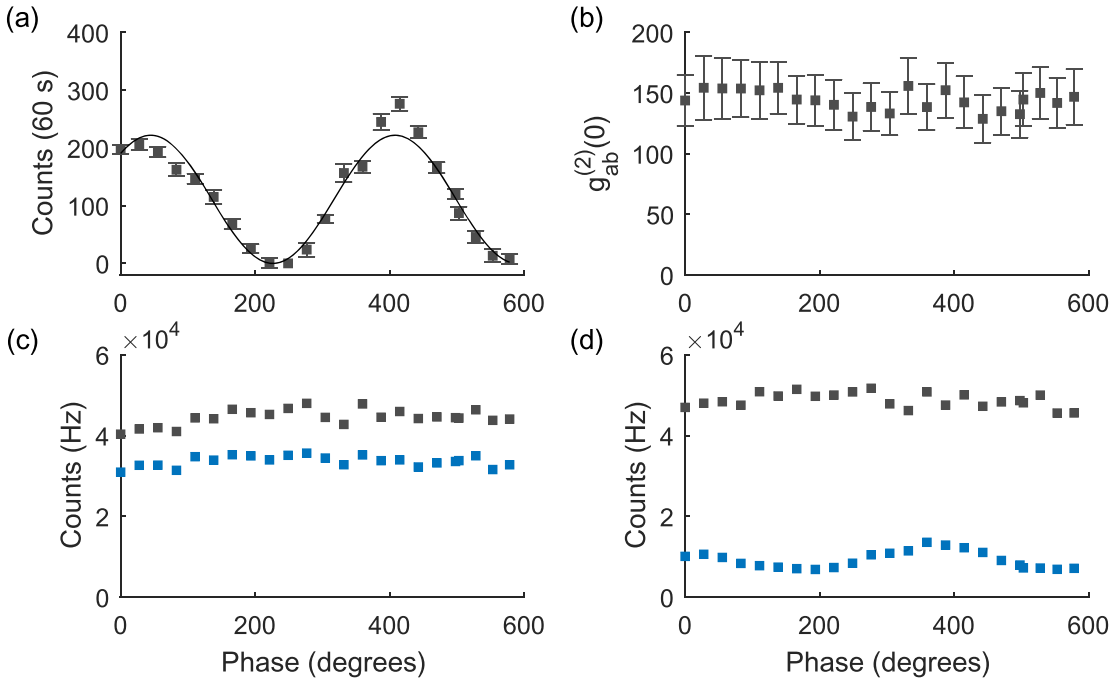

Figure 7. Time–energy entanglement measurement of 1310 nm photon pairs at presence of 1550 nm pump. (a) Franson visibility fringe of the 'short–short' and 'long–long' coincidence interference for photons pairs generated near 1310 nm. (b) Second-order cross-correlation function, related to the coincidences-to-accidentals ratio (CAR) for photon pairs generated near 1550 nm. (c) Measured singles count rates for signal and idler photons near 1310 nm. (d) Measured singles count rates for signal and idler photons near 1550 nm.

time, $g^{(2)}_{SI}(0)$, of 1310 nm photon pair as a function of phase tuning on the DLIs, whose lack of variation shows that the correlation in the 1310 nm photon pairs was maintained during the measurements.

Similarly, the Franson visibility measurement results for 1310 nm photon pairs were shown in figure 7. For the measurement in figure 7(d), one of the fiber connections in the filter assembly broke and was manually spliced, incurring a 5 dB differential transmission loss (of one channel with the respect to the other), which does not affect the interpretation that $g^{(2)}(0)$ of the signal-idler photon pair generated at 1550 nm was invariant during the Franson measurement at 1310 nm. The observed fringe in figure 7(a) shows a fitted visibility of $97.4 \pm 13.3\%$, which also evidences time–energy entanglement of the 1310 nm photons. In both cases, the flat singles rates (versus phase), shown in figures 6(c), (d) and 7(c), (d), show the absence of single-photon interference, as desired [43, 44].

The high visibilities measured here in the dual-pump case are similar quantitatively to the values we reported previously for the single-pump case [24]. Taken together, figures 6 and 7 confirm that the energy–time entanglement properties of the pairs were maintained during the presence of the second pump.

4. Conclusion

The measurement results reported here show the feasibility of using an appropriately-designed silicon microring to generate entangled photon pairs at the two optical fiber communication bands (1310 and 1550 nm) simultaneously. The signal-idler cross-correlation and time–energy entanglement of photon pairs generated by individual pumps were maintained during the presence of the second pump. These results lead the way to spectrally-multiplexed time–energy entanglement generation, which is a distinct step beyond multiplexed correlated-photon generation, and pair generation at distinct wavelength bands. Although the photons share the same physical medium (i.e., the silicon microring resonator), and there must be some correlations between the spectral bands (induced, for example, by electronic carrier effects in the semiconductor), we see that they do not destroy entanglement, and there were no measurable cross-correlations between the SFWM process across the bands. These conclusions may be different if the properties of the microring were to be substantially changed. For example, in micro-resonators with significantly higher Q values, the optical pump intensity of the recirculating field is higher. For lower Q values, the pair generation rate may be too small, thus requiring stronger pump powers. In either case, the racetrack and/or directional coupler may be affected more strongly by thermal and free-carrier induced shifts, beyond the scope of mitigation of the reverse-biased diode, and lead to potential impairments, such as cross-pump correlations.

In the process of performing these measurements, we also measured a CAR of 19 000 which is the highest CAR value yet reported for pair generation in silicon photonic microrings, at any wavelength. Recently, we reported on the high brightness (number of pairs per second normalized by the pump power) in these structures [24]. Therefore, silicon microfabrication should be viewed not only a low-cost manufacturing platform, but as a pathway to achieving high performance in optically-pumped pair generation devices with the appropriate design. Further improvements are being considered in the device and experiment, including: (a) improved design of the microring to maintain Q-factors while supporting higher pump power (i.e., further increasing the overall pair generation rate); (b) usage of filters with higher isolation especially at wavelengths far removed from the transmission peak (i.e., larger finesse); and (c) integration of the various components shown in figure 2 to reduce interface and coupling losses.

Acknowledgments

We gratefully acknowledge the financial support from National Science Foundation (NSF) (ECCS-1201308, EFMA-1640968 'ACQUIRE: Microchip Photonic Devices for Quantum Communication over Fiber').

ORCID iDs

Chaoxuan Ma https://orcid.org/0000-0002-0848-8093

References

[1] Hall M A, Altepeter J B and Kumar P 2009 *Opt. Express* **17** 14558–66
[2] Hall M A, Altepeter J B and Kumar P 2011 *New J. Phys.* **13** 105004
[3] Migdall A, Polyakov S V, Fan J and Bienfang J C 2013 *Single-Photon Generation and Detection: Physics and Applications* vol 45 (New York: Academic)
[4] Fiorentino M, Voss P L, Sharping J E and Kumar P 2002 *IEEE Photonics Technol. Lett.* **14** 983–5
[5] Kwiat P G, Waks E, White A G, Appelbaum I and Eberhard P H 1999 *Phys. Rev.* A **60** R773–6
[6] Lobino M *et al* 2011 *Appl. Phys. Lett.* **99** 081110
[7] Brida G *et al* 2012 *Appl. Phys. Lett.* **101** 221112
[8] Harder G, Ansari V, Brecht B, Dirmeier T, Marquardt C and Silberhorn C 2013 *Opt. Express* **21** 13975–85
[9] Bock M, Lenhard A, Chunnilall C and Becher C 2016 *Opt. Express* **24** 23992–4001
[10] Sharping J E, Lee K F, Foster M A, Turner A C, Schmidt B S, Lipson M, Gaeta A L and Kumar P 2006 *Opt. Express* **14** 12388–93
[11] Clemmen S, Huy K P, Bogaerts W, Baets R G, Emplit P and Massar S 2009 *Opt. Express* **17** 16558–70
[12] Azzini S, Grassani D, Strain M J, Sorel M, Helt L G, Sipe J E, Liscidini M, Galli M and Bajoni D 2012 *Opt. Express* **20** 23100–7
[13] Davanco M, Ong J R, Shehata A B, Tosi A, Agha I, Assefa S, Xia F, Green W M J, Mookherjea S and Srinivasan K 2012 *Appl. Phys. Lett.* **100** 261104
[14] Harris N C, Grassani D, Simbula A, Pant M, Galli M, Baehr-Jones T, Hochberg M, Englund D, Bajoni D and Galland C 2014 *Phys. Rev.* X **4** 041047
[15] Liu M T, Huang Y and Lim H C 2013 Generation of O-band heralded single-photons using a silicon wire waveguide *2013 Conf. on Lasers and Electro-Optics Pacific Rim (CLEOPR)* (Piscataway, NJ: IEEE) 1–2
[16] Gentry C M *et al* 2015 *Optica* **2** 1065–71
[17] Jiang W C, Lu X, Zhang J, Painter O and Lin Q 2015 *Opt. Express* **23** 20884–904
[18] Savanier M, Kumar R and Mookherjea S 2016 *Opt. Express* **24** 3313–28
[19] Lu X, Rogers S, Gerrits T, Jiang W C, Nam S W and Lin Q 2016 *Optica* **3** 1331–8
[20] Silverstone J W *et al* 2014 *Nat. Photon.* **8** 104
[21] Matsuda N, Le Jeannic H, Fukuda H, Tsuchizawa T, Munro W J, Shimizu K, Yamada K, Tokura Y and Takesue H 2012 *Sci. Rep.* **2** 817
[22] Wang X, Ma C, Kumar R, Doussiere P, Jones R, Rong H and Mookherjea S 2017 Photon pair generation using silicon photonic microring and hybrid laser *Conf. on Lasers and Electro-Optics* (Optical Society of America) p JTh5C.6 (http://osapublishing.org/abstract.cfm?URI=CLEO_SI-2017-JTh5C.6)
[23] Schuck C, Pernice W and Tang H 2013 *Appl. Phys. Lett.* **102** 051101
[24] Ma C, Wang X, Anant V, Beyer A D, Shaw M D and Mookherjea S 2017 *Opt. Express* **25** 32995–3006
[25] Savanier M, Kumar R and Mookherjea S 2015 *Appl. Phys. Lett.* **107** 131101
[26] Savanier M and Mookherjea S 2016 *Appl. Phys. Lett.* **108** 251102
[27] Ma C, Sacher W D, Tang Z, Mikkelsen J C, Yang Y, Xu F, Thiessen T, Lo H K and Poon J K S 2016 *Optica* **3** 1274–8
[28] Cai H *et al* 2017 *Opt. Express* **25** 12282–94
[29] Sibson P, Kennard J E, Stanisic S, Erven C, O'Brien J L and Thompson M G 2017 *Optica* **4** 172–7
[30] Choi I, Young R J and Townsend P D 2011 *New J. Phys.* **13** 063039
[31] Eraerds P, Walenta N, Legré M, Gisin N and Zbinden H 2010 *New J. Phys.* **12** 063027
[32] Li X, Voss P L, Sharping J E and Kumar P 2005 *Phys. Rev. Lett.* **94** 053601
[33] Liu M T and Lim H C 2013 *Opt. Express* **21** 30358–69
[34] De Riedmatten H, Marcikic I, Tittel W, Zbinden H and Gisin N 2003 *Phys. Rev.* A **67** 022301
[35] Alibart O, Ostrowsky D B, Baldi P and Tanzilli S 2005 *Opt. Lett.* **30** 1539–41
[36] Meany T, Ngah L A, Collins M J, Clark A S, Williams R J, Eggleton B J, Steel M, Withford M J, Alibart O and Tanzilli S 2014 *Laser Photonics Rev.* **8** L42–6
[37] Alibart O, Ostrowsky D B, Baldi P and Tanzilli S 2005 *Opt. Lett.* **30** 1539–41
[38] Aguinaldo R, Shen Y and Mookherjea S 2012 *IEEE Photonics Technol. Lett.* **24** 1242–4

[39] Steidle J A, Fanto M L, Tison C C, Wang Z, Preble S F and Alsing P M 2015 High spectral purity silicon ring resonator photon-pair source *Proc. SPIE* **9500** 950015
[40] Savanier M, Ozanam C, Lanco L, Lafosse X, Andronico A, Favero I, Ducci S and Leo G 2013 *Appl. Phys. Lett.* **103** 261105
[41] Yariv A 2000 *Electron. Lett.* **36** 321–2
[42] Xiong C, Helt L, Judge A, Marshall G, Steel M, Sipe J and Eggleton B 2010 *Opt. Express* **18** 16206–16
[43] Franson J D 1989 *Phys. Rev. Lett.* **62** 2205
[44] Kwiat P G, Steinberg A M and Chiao R Y 1993 *Phys. Rev.* A **47** R2472
[45] Harada K i, Takesue H, Fukuda H, Tsuchizawa T, Watanabe T, Yamada K, Tokura Y and Itabashi S I 2008 *Opt. Express* **16** 20368–73
[46] Grassani D, Azzini S, Liscidini M, Galli M, Strain M J, Sorel M, Sipe J E and Bajoni D 2015 *Optica* **2** 88–94
[47] Wakabayashi R, Fujiwara M, Ichiro Y K, Nambu Y, Sasaki M and Aoki T 2015 *Opt. Express* **23** 1103–13
[48] Suo J, Dong S, Zhang W, Huang Y and Peng J 2015 *Opt. Express* **23** 3985–95
[49] Kumar R, Savanier M, Ong J R and Mookherjea S 2015 *Opt. Express* **23** 19318–27
[50] Mazeas F *et al* 2016 *Opt. Express* **24** 28731–8